Density change upon solidification of silicon cast irons

Jacques Lacaze, Jon Sertucha, Urko de la Torre

Density change upon solidification of silicon cast irons

Jacques LACAZE[1], Jon SERTUCHA[2], Urko de la TORRE[2]

1. CIRIMAT, Université de Toulouse, CS 44362, 31030 Toulouse, France

2. Azterlan, Basque Research and Technology Alliance, Aliendalde Auzunea 6, E-48200 Durango (Bizkaia), Spain.

Corresponding author J. Lacaze: Jacques.lacaze@ensiacet.fr

Abstract

Amongst the possible defects that can appear during casting, voids due to solidification shrinkage is certainly the most usual and important in the case of cast irons. For any predicting work, the knowledge of the density of the phases of interest, namely liquid, austenite and graphite, is a prerequisite. The density of liquid and austenite in silicon cast irons are here assessed as function of composition and temperature based on literature review. Estimate of theoretical expansion upon solidification are then derived for lamellar and spheroidal graphite cast irons and compared to reported experimental values obtained in near-equilibrium conditions.

Keywords: cast iron, volume change, solidification, density

Competing Interests: The authors declare they have no competing interest.

1. Introduction

Volume changes during solidification and cooling of cast alloys have long been the primary concern of foundry men. Since most casting defects are generated during solidification, special attention is paid to the volume changes between liquid and solid which, in the case of cast irons, is known to depend on the shape of the precipitating graphite. Volume changes are quantitatively expressed in terms of specific volume, v, or its inverse the density, ρ, of the related phases, namely liquid, austenite and graphite.

As a preliminary step before considering the formation of casting defects, the objective of the present work is to express the density of cast irons when free of voids. This can be called the theoretical density, and is thought to depend solely on temperature and composition. Further, the fact that cast irons are iron-rich alloys led to consider first the properties of pure iron and then to look for the effect of additions, mostly carbon and silicon. This has been done successively for liquid and austenite. Theoretical density change associated with cast iron solidification is then calculated and discussed. An explanation to the difference in the propensity of lamellar graphite irons (LGI) and spheroidal graphite irons (SGI) to form shrinkage defects is suggested.

2. Density of cast iron melts

Jablonka et al. [1] have provided a review of data for pure iron and Fe-C alloys from liquid state to room temperature. The information in this review was used by Miettinen [2] to establish the properties of steels, i.e. accounting for the effect of Si, Mn, Cr, Mo and Ni in addition to carbon. In the Jablonka's review, one of the reference works on liquid iron and its alloys is that of Lucas [3] who investigated the effect of carbon, silicon and phosphorus. Much weight will be put on the results of this latter study in reviewing other available works on binary and ternary alloys. Validation of this selective approach will be gained when comparing predictions with experimental values for liquid cast irons, in particular those of the extensive study by Ash and Saeger [4].

For metallic melts, the most usual methods for density evaluation are weighing, sessile drop and maximum bubble pressure, while newer methods such as electrostatic and electromagnetic levitation do not appear to have been used for the alloys involved in the present work. Using the pressure bubble technique in which a capillary is inserted at two heights in the melt to get rid of surface tension effects, Lucas [3] arrived at the following relation for the specific volume of pure liquid iron (all specific volumes will be expressed in $cm^3.g^{-1}$):

$$v_{Fe}^{liq} = 0.1421 + 30.7 \cdot 10^{-6} \cdot (T_K - 1809) \quad (1)$$

where T_K is the temperature in Kelvin.

The second term in Eq. (1) is very small when compared to the constant term, meaning that a good estimate of the density of pure liquid iron is directly obtained as (all densities will be expressed in $g \cdot cm^{-3}$):

$$\rho_{Fe}^{liq} = 7.037 - 0.216 \cdot 10^{-3} \cdot (T_K - 1809) \quad (1')$$

However, Lucas recognized that the temperature coefficient in Eq. (1) was much higher than the value reported in other works, possibly because of the limited temperature range in which was investigated the pure iron. This means that the temperature coefficient in Eq. (1') is too low compared to most reported values. Accordingly, the temperature coefficient considered in the present work will be taken from the assessment by Yoshikawa [5]:

$$\rho_{Fe}^{liq} = 7.035 - 0.926 \cdot 10^{-3} \cdot (T_K - 1811) = 8.459 - 0.926 \cdot 10^{-3} \cdot T_C \quad (2)$$

where T_C is the temperature in Celsius.

It is worth comparing this expression to that assessed by Jablonka et al. that is:

$$\rho_{Fe}^{liq} = 8.319 - 0.91 \cdot 10^{-3} \cdot T_C \quad (2')$$

The difference between the values given by (2) and (2') is zero at the melting point of iron (1538°C) and is less than 0.4% at 1200°C thus sustaining the choice of using Eq. (2) in the following.

2.1. Fe-C liquid alloys

A series of experiments for carbon content between 0 and 4.27 wt.% has been carried out by Lucas [3] using again the pressure bubble technique. The experiments were done between 1200°C and 1600°C for the highest carbon content and in a more limited range for less dilute alloys. The carbon content was checked on metal sucked out from the melt both before and after the pressure measurement. Lucas showed in graphs all the individual measurements but reported in tables interpolated values that are those used in this work. As an example, both individual and interpolated results at 1600°C on the whole series of alloys are plotted in Fig. 1 where it is seen that this selection of interpolated values is appropriate. Fig. 1 shows a curvature at high carbon content that could be described by a second order polynomial:

$$\rho_{Fe-C}^{liq}(1600°C) = 6.937 - 0.0735 \cdot w_C + 0.00659 \cdot w_C^2 \quad (3)$$

where w_C is the carbon content (wt.%).

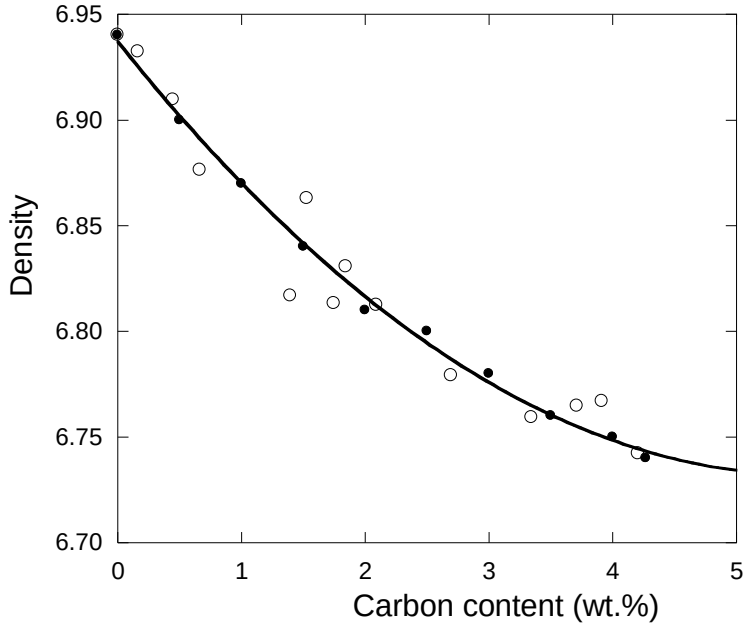

Figure 1. Experimental density results of Lucas for Fe-C alloys at 1600°C, with the open circles being the measurements plotted in his figure 6 and the solid circles the interpolated values listed in his table VII. The solid curve is the best fit polynomial given by Eq. (3).

The value of 6.937 for pure iron at 1600°C indicated by Eq. (3) is in between those given by Eq. (2) and Eq. (2'). Then, introducing Eq. (2) in Eq. (3) and checking for other Lucas' results evidenced that the effect of carbon was dependent on temperature. Such a temperature dependence has been considered by Jimbo and Cramb [6] when analyzing their own data and led them to add a term function of w_C in the temperature coefficient. Keeping the effect of temperature for pure iron given by Eq. (2) and introducing the effect of carbon according to Eq. (3), Lucas' results lead to express the density of liquid Fe-C alloys as:

$$\rho_{Fe-C}^{liq} = 6.99 - 0.0735 \cdot w_C + 0.00659 \cdot w_C^2 - (0.926 - 0.05 \cdot w_C) \cdot 10^{-3} \cdot (T_K - 1811) \qquad (4)$$

$$\rho_{Fe-C}^{liq} = 8.414 - 0.1504 \cdot w_C + 0.00659 \cdot w_C^2 - (0.926 - 0.05 \cdot w_C) \cdot 10^{-3} \cdot T_C \qquad (4')$$

It is noteworthy that the use of the melting temperature of iron at 1811 K as the pivotal temperature in equation (4) has no physical significance regarding the thermal effect of carbon, and is only used here for its convenience. Calculated density values for all Fe-C alloys studied by Lucas are compared to experimental ones in Fig. 2 where a really good agreement is observed, demonstrating that the introduction of the correction due to carbon in the temperature coefficient was essential for a proper description of these results.

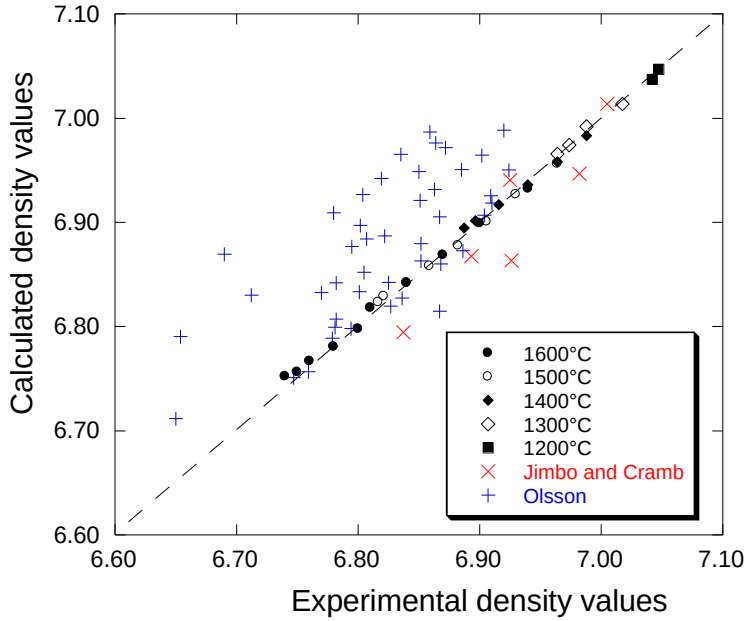

Figure 2. Comparison of experimental data to values calculated using Eq. (4). The dashed line is the bisector. Data from Lucas [3] are interpolated values listed in his Table VIII for alloys with 0 to 4.27 wt.% C and temperature ranging in between 1200°C and 1600°C. Data from Jimbo and Cramb [6] are for Fe-1.91C and Fe-3.91C (wt.%) at 1600°C. Values from Olsson [7] are for alloys with 0.1 to 2.7 wt.% C and temperature between 1350°C and 1700°C (his table II) and for Fe-C alloy with 2.7 wt.% C at 1350°C, 1400°C and 1450°C (his figure 7).

Jimbo and Cramb [6] made a couple of measurements of the density of Fe and of Fe-C alloys at 1.91 and 3.91 wt.% carbon using the sessile drop technique. Depending on the carbon content, the experiments were carried out at temperature ranging between 1250°C and 1550°C. The results have also been plotted in Fig. 2 were they are seen to be quite satisfactorily reproduced though apparently scattered.

Using the bubble technique, Olsson [7] carried out an extensive investigation on the effect of carbon, silicon and molybdenum on the density of liquid Fe. As for Fe-C alloys, emphasis was put on the low carbon contents (<1 wt.%) though an alloy at 1.5 and another at 2.7 wt.% C were investigated. All his results for Fe-C alloys have been reported in Fig. 2 where it is seen that the experimental values are quite scattered and systematically lower than the calculated ones, though the difference is at most of 2.5%. This difference is certainly in relation with the fact that the density for pure iron reported by Olsson is at all temperatures lower than the assessed value.

2.2. Fe-P and Fe-C-P alloys

The only results that are known are again due to Lucas who studied a Fe-P alloy with 2.25 wt.% P and a Fe-C-P alloy with 1.9 wt.% C and 1.8 wt.% P. The slope of the change in density with temperature for the Fe-P alloy was similar to that for Fe-C alloy, suggesting a simple compositional effect. However, in the case of the Fe-C-P alloy, the slope differed and accounting for the carbon content with Eq. (3) was not sufficient, demonstrating that the temperature term should also contain a term for phosphorus. Attempts to describe in a simple way the behavior of the two P-bearing alloys turned out to be impossible so that it was decided to put emphasis on the Fe-C-P alloy and the following equation was obtained:

$$\rho^{liq}_{Fe-C-P} = 6.99 - 0.0735 \cdot w_C + 0.00659 \cdot w_C^2 - 0.0475 \cdot w_P - (0.926 - 0.05 \cdot w_C - 0.08 \cdot w_P) \cdot 10^{-3} \cdot (T_K - 1811) \quad (5)$$

$$\rho^{liq}_{Fe-C-P} = 8.414 - 0.1504 \cdot w_C + 0.00659 \cdot w_C^2 - 0.1705 \cdot w_P - (0.926 - 0.05 \cdot w_C - 0.08 \cdot w_P) \cdot 10^{-3} \cdot T_C \quad (5')$$

Data for Fe-P and Fe-C-P alloys are plotted in Fig. 3 where it is seen that calculated values for the Fe-P alloy are at most 0.05 g·cm^{-3} higher than the experimental ones, i.e. differ by less than 1%. Furthermore, it will be shown with the analysis of data for cast irons that the choice made here is relevant.

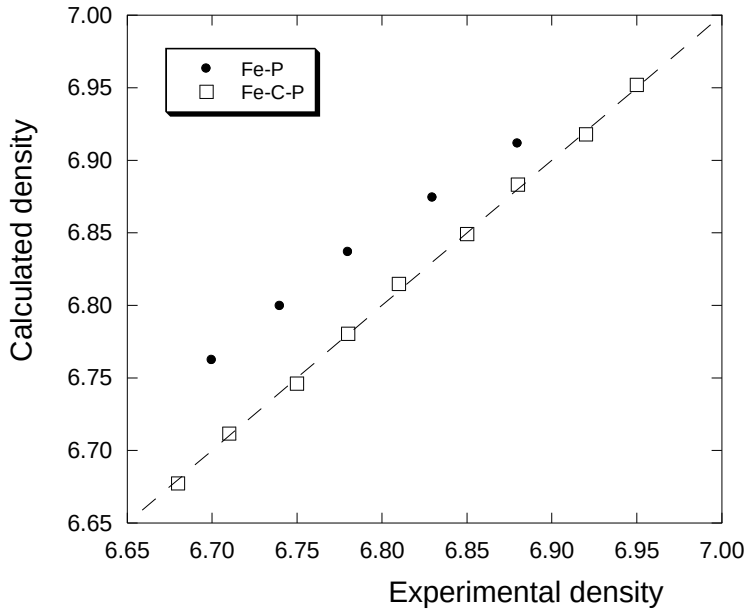

Figure 3. Comparison of experimental data for Fe-P and Fe-C-P alloys with ones calculated with Eq. (5). The dashed line is the bisector.

2.3. Fe-Si alloys

There are several studies on the density of liquid Fe-Si alloys for application to geology, meaning that most of them are for high silicon contents. On the contrary, limited data are available for the range of interest to steels and cast irons, i.e., silicon content lower than 5 wt.% [3, 7, 8]. In works dealing with the whole range of composition, values for alloys with less than 20 wt.% Si could be found in a few works [5, 9, 10, 11]. All relevant data are listed in Annex A and the most numerous values corresponding to temperatures between 1450°C and 1600°C are shown in Fig. 4, with emphasis on the data for 1550°C which are represented by solid symbols while others are represented with open symbols. With the exception of the measurements from Gertman and Gel'd [9], all values are reasonably consistent between each other though scattered. The fact that Olsson's values are here well in line with other data suggests that the bias on Fe-C alloys observed in Fig. 2 could have been due to a slight oxidation of the melt that is strongly decreased in the presence of silicon.

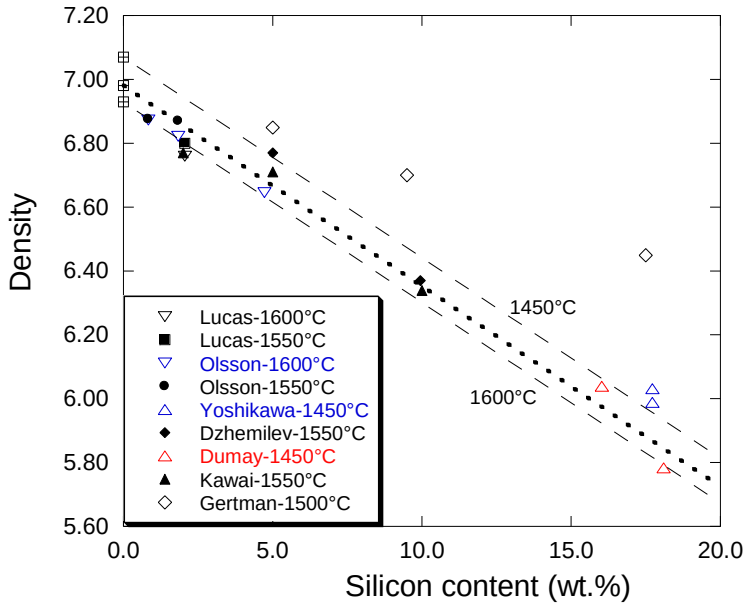

Figure 4. Density values for Fe-Si alloys at temperature between 1450°C and 1600°C. The dashed lines run parallel to each other from the reference values calculated with Eq. (4) at w_C=0, with the bold one corresponding to 1550°C.

The lines in Fig. 4 have been drawn parallel to each other starting from the reference values calculated with Eq. (4) at w_C=0. The bold dotted line appears as the best fit to data at 1550°C. These lines give a silicon coefficient of -0.063 g.cm^{-3}/wt.% quite close to the one of -0.065

g.cm^{-3}/wt.% considered by Jablonka et al. This leads to write the density of iron-rich liquid Fe-Si alloys as:

$$\rho_{Fe-Si}^{liq} = 6.99 - 0.063 \cdot w_{Si} - 0.926 \cdot 10^{-3} \cdot (T_K - 1811) \qquad (6)$$

$$\rho_{Fe-Si}^{liq} = 8.414 - 0.063 \cdot w_{Si} - 0.926 \cdot 10^{-3} \cdot T_C \qquad (6')$$

Fig. 5 shows the comparison of calculated versus experimental values for all data listed in Table 2 (Appendix A) but those from Gertman and Gel'd that appear strongly biased in Fig. 4. It is seen that Eq. (6) reproduces most of the experimental data within ±0.1 g·cm^{-3}, that is ±1.5% of the density value. The results of Lucas and those of Olsson for 4.73 wt.% Si could suggest a slight temperature effect of silicon as postulated by Miettinen [2] assuming an ideal behavior of the Fe-Si alloys. However, analysis of the experimental results in Fig. 5 did not give any relevant relation on the statistical point of view.

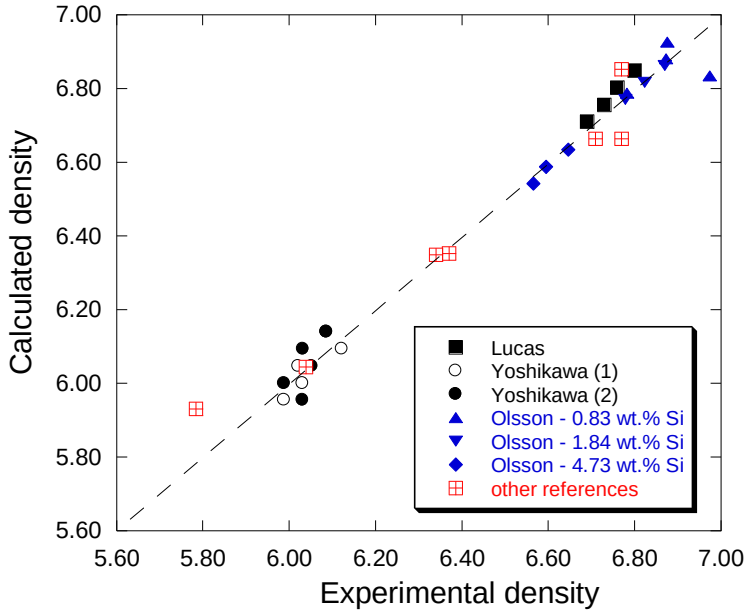

Figure 5. Comparison of experimental data for Fe-Si alloys to values calculated using Eq. (6). The dashed line is the bisector. "Other references" stands for values listed in Table 2 from Dzhemilev et al. [10], Kawai et al. [11] and Dumay and Cramb [8].

2.4. Fe-C-Si alloys and cast irons

It will be considered that other metallic elements that are present at low level such as Cu and Mn –that are close to Fe in the periodical table of elements- do not to affect density of liquid cast irons. Merging the above equations, the density of liquid Fe-C-Si alloys and cast irons is thus expressed as:

$$\rho^{liq} = 6.99 - 0.0735 \cdot w_C + 0.00659 \cdot w_C^2 - 0.0475 \cdot w_P - 0.063 \cdot w_{Si} - (0.926 - 0.05 \cdot w_C - 0.08 \cdot w_P) \cdot 10^{-3} \cdot (T_K - 1811) \quad (7)$$

$$\rho^{liq} = 8.414 - 0.1504 \cdot w_C + 0.00659 \cdot w_C^2 - 0.1705 \cdot w_P - 0.063 \cdot w_{Si} - (0.926 - 0.05 \cdot w_C - 0.08 \cdot w_P) \cdot 10^{-3} \cdot T_C \quad (7')$$

There are very little data on Fe-C-Si alloys. In their studies on surface tension of Fe-C-Si alloys, Kawai et al. [11] reported density values for Fe-Si alloys that were considered above and also values for Fe-C-Si alloys with C at 1 wt.% and 3 wt.% and Si between 1 wt.% and 10 wt.%. Attempts to use these values showed them to be inconsistent and were thus disregarded, in the same way their surface tension values had to be disregarded in a previous study [12]. At higher silicon content, Yoshikawa [5] studied the density and surface tension of the same Fe-Si alloys as those mentioned in the previous section but after having saturated them with carbon. His Fe-30 at.% Si alloy was saturated in graphite crucible; the corresponding compositions have been recalculated using TCFE-8 [13] and are listed in Appendix B together with experimental density values. Predictions using Eq. (7) are also given in Table 3 and show to be too high by up to 0.2 $g \cdot cm^{-3}$ possibly because the simple linear relation is insufficient at such high silicon contents.

The most extensive work on cast irons is due to Ash and Saeger [4] who used a weighing method. They investigated alloys with carbon between 2 wt.% and 3.75 wt.%, silicon in the range 0.85 wt.% to 2.9 wt.% and phosphorus up to 0.7 wt.%, for temperature varying between 1220°C and 1510°C. All their data are presented in Appendix C where the calculations carried out without and with phosphorus are shown and differentiated according to the composition of the various alloys. The comparison of these two set of calculations showed that accounting for phosphorus is important. In Fig. 6, experimental density values from Ash and Saeger study are represented versus the calculated ones with the same symbol for all, i.e. not differentiated as done in Appendix C. It is seen in Fig. 6 that the experimental values are reproduced at better than 0.05 $g \cdot cm^{-3}$, i.e., at better than 0.7%.

Other results worth of mention are those from Kusakawa et al. [14] who also used a weighing method. These authors compared density for one target hypereutectic composition and various melt treatments, namely no treatment, Ca-Si and Fe-Si-Mg spheroidizing treatments. Their graphs show that for carbon at 3.7-3.8 wt.% and silicon at 2.6-2.7 wt.%, the density of the liquid does not depend on the treatment and varies from about 6.90 at 1355°C to 6.77 at 1475°C. On the contrary, below a temperature associated with the graphite liquidus,

differences appeared with the melt treatment. The values for the Ca-Si treated melts are shown in Fig. 6 with small black dots where they are seen to be lower by 0.10-0.15 than those from Ash and Saeger. It was however realized that the liquidus temperature reported by these authors at 1365°C is about 140°C above the expected graphite liquidus for their target composition. Such a difference suggests that a significant cooling of the melt occurred when poured in the calibrated cup used for density evaluation. Though admittedly a very rough way of doing, this value of 140°C was used to correct the measurement temperature. The corresponding calculated values are shown with large red dots in Fig. 6 where it is found that good agreement is then obtained with the experimental data from Ash and Saeger.

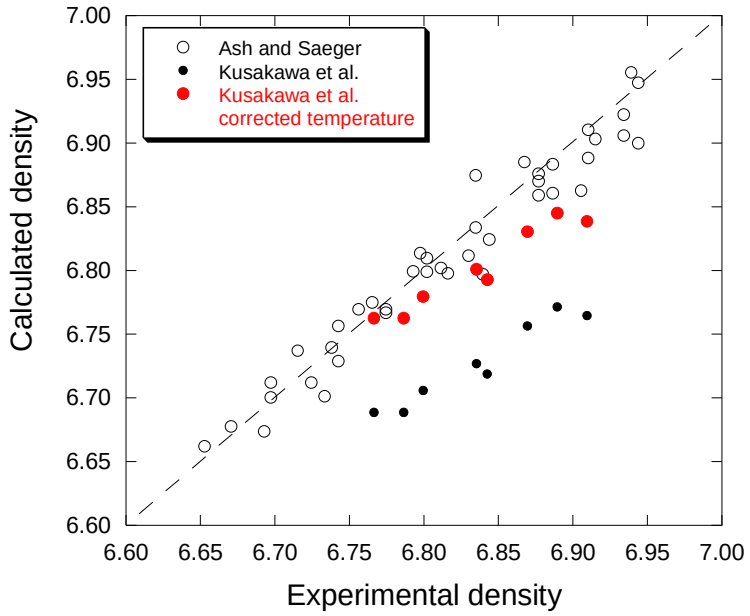

Figure 6. Calculated versus experimental density values of cast irons

2.5. Effect of temperature and coefficient of thermal expansion

For many purposes, these are the temperature effects that are considered that, for the density, is readily obtained from Eq. (7) as ($g \cdot cm^{-3} \cdot °C^{-1}$):

$$\frac{d\rho^{liq}}{dT} = -(0.926 - 0.05 \cdot w_C - 0.08 \cdot w_P) \cdot 10^{-3} \qquad (8)$$

This gives -0.751 $kg \cdot m^{-3} \cdot °C^{-1}$ for a cast iron with 3.5 wt.% carbon and no phosphorus. This value is in the middle of the range of values reviewed by Hellström et al. [15], in excellent agreement with those by Ash and Saeger and by Lucas as expected.

With the density being $\rho = m / V$, where m is the mass and V the volume of a sample, the linear thermal expansion coefficient β is given as:

$$\beta = \frac{1}{3}\cdot\frac{1}{V}\cdot\frac{dV}{dT} = \frac{1}{3}\cdot\frac{m}{V}\cdot\frac{d\left(1/\rho^{liq}\right)}{dT} = \frac{-1}{3}\cdot\frac{\left(d\rho^{liq}/dT\right)}{\rho^{liq}} \qquad (9)$$

that can be readily calculated using Eq. (7) and Eq. (8).

3. Austenite

There are three available methods for evaluating the density of austenite: measuring the volume to get the specific volume, measuring the parameter of the fcc lattice and dilatometry that however needs a reference value. Lucas [16] used the first method for pure iron and reported 4 measures of the change of volume in the γ-range (between 1000°C and 1300°C). From these, he proposed a linear relation for the specific volume of pure fcc Fe ($cm^3 \cdot g^{-1}$):

$$v_{Fe}^{\gamma} = 0.1221 + 9.7\cdot 10^{-6}\cdot(T_C - 20) \qquad (10)$$

that can be written as well as:

$$v_{Fe}^{\gamma} = 0.1219 + 9.7\cdot 10^{-6}\cdot T_C \qquad (10')$$

Lucas compared his results with those from other studies, in particular the results from Basinski et al. [17] who measured the lattice parameters, and concluded to a good agreement between the various sets of values when considering the relative volume change.

As a matter of fact, measurement of the fcc lattice parameter seems to be the most straightforward way of characterizing the change with temperature and composition of the fcc lattice. Combining results from Basinski et al. [17] and others for pure Fe, Ridley and Stuart [18] for Fe-C alloys and Cockett and Davis [19] for Fe-Si alloys, Chen et al. [20] offered the following relation for the fcc lattice parameter (all lattice values in Å):

$$a^{\gamma} = 3.63 + 8.055\cdot 10^{-5}\cdot(T_C - 727) + \left\{0.0296 - 2.96\cdot 10^{-6}\cdot(T_C - 727)\right\}\cdot w_C - 0.001\cdot w_{Si} \qquad (11)$$

This equation is at slight change with that assessed by Dietrich and Lesoult [21] who expressed the effect of carbon on the specific mass using a second order polynomial in carbon. The results from Basinski et al. and of Ridley and Stuart were picked up from the figure 1 in the work by these latter authors and are reproduced in Fig. 7-a. It is worth stressing that the high-temperature X-ray camera used by Ridley and Stuart was calibrated using the data of Basinski et al. for pure iron. All the results in Fig. 7-a were processed using JMP statistical software package which led without any ambiguity to a second order polynomial in carbon that is written (Å):

$$a^{\gamma} = 3.57344 + 8.0344\cdot 10^{-5}\cdot T_C + 0.01865\cdot w_C + 0.007019\cdot w_C^2 \qquad (12)$$

Calculated data are compared in Fig. 7-b to experimental values shown in Fig. 7-a and it is seen how excellent the fit obtained with Eq. (12) is.

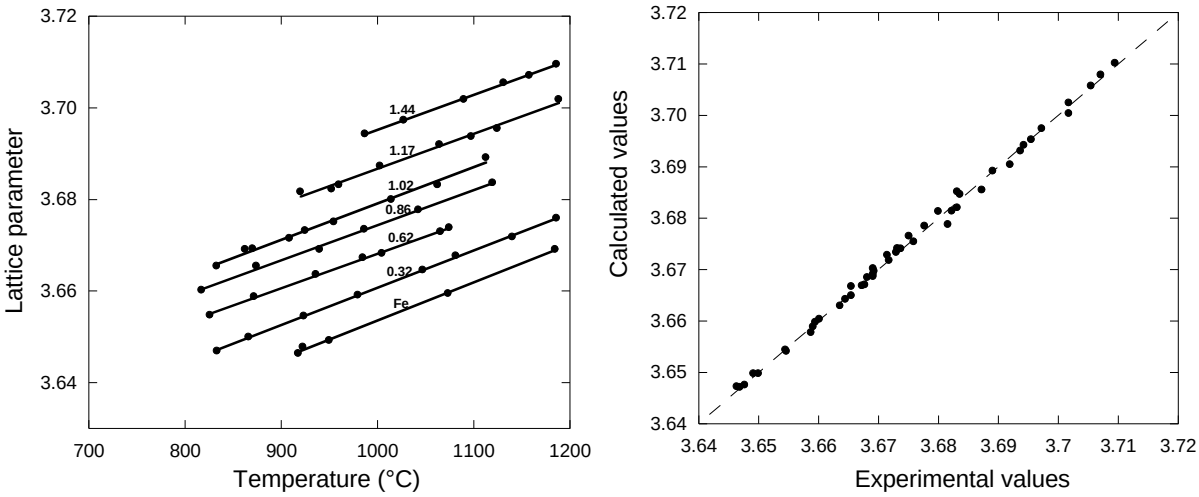

Figure 7. a: Effect of temperature on the fcc lattice parameter (Å) for various carbon contents that are indicated in wt.% along the lines that are the best fit lines. Data from Fig. 1 in Ridley and Stuart [18] with those for pure Fe originally from Basinski et al. [17]. b: Correlation between experimental values in a and values calculated using Eq. (12). The dashed line is the bisector.

Accepting the term in silicon from Eq. (11) and denoting the constant term as $a^{\gamma,0} = 3.57344$ gives the following expression:

$$a^{\gamma} = a^{\gamma,0} + 8.0344 \cdot 10^{-5} \cdot T_C + 0.01865 \cdot w_C + 0.007019 \cdot w_C^2 - 0.001 \cdot w_{Si} \qquad (13)$$

It is worth stressing that silicon contracts the austenite lattice, while carbon increases it.

The classical calculation of the specific volume from the lattice parameter consists to evaluate the molar volume, V_m^{γ}, and the molar mass, M_m^{γ}, of the fcc structure, i.e., the crystallographic structure made up of substitutional elements (Fe, Si, etc.). The molar volume is such that each substitutional site pertains to four elementary volumes so that:

$$V_m^{\gamma} = \frac{x_{subst} \cdot N_A \cdot \left(a^{\gamma}\right)^3}{4} \qquad (14)$$

In this relation, N_A is the Avogadro's number and x_{subst} is the molar fraction of substitutional sites of the alloy. For a ternary Fe-C-Si alloy, x_{subst} is expressed as:

$$x_{subst} = \frac{x_{Fe} + x_{Si}}{x_{Fe} + x_{Si} + x_C} = x_{Fe} + x_{Si} = 1 - x_C \qquad (15)$$

where x_i is the molar fraction of element i.

The molar mass is simply given as:

$$M_m^{\gamma} = x_{Fe} \cdot M_{Fe} + x_{Si} \cdot M_{Si} + x_C \cdot M_C \qquad (16)$$

in which M_i is the molar mass of element i.

Applying Eq. (13) and Eq. (14) for pure iron, i.e. with x_{Fe}=1, leads to the following expression for the molar volume ($cm^3 \cdot mol^{-1}$):

$$V_m^{\gamma} = 6.8697 \cdot (1 + 2.2484 \cdot 10^{-5} \cdot T_C)^3 \qquad (17)$$

Noting that the second term between the brackets is very small, the molar volume can be approximated as:

$$V_m^{\gamma} \approx 6.8697 \cdot (1 + 6.745 \cdot 10^{-5} \cdot T_C) = V_m^{\gamma,0} \cdot (1 + 6.745 \cdot 10^{-5} \cdot T_C) \qquad (17')$$

where $V_m^{\gamma,0} = N_A \cdot \left(a^{\gamma,0}\right)^3 / 4 = 6.8697\ cm^3.mol^{-1}$

By dividing the approximate expression (17') of the molar volume by M_{Fe}=55.845 $g \cdot mol^{-1}$, the specific volume of pure fcc Fe is given as ($cm^3.g^{-1}$):

$$v_{Fe}^{\gamma} = 0.1230 + 8.297 \cdot 10^{-6} \cdot T_C \qquad (18)$$

Eq. (18) appears to slightly differ from Eq. (10'). However, the density of pure fcc Fe calculated at 1150°C changes from 7.516 for Eq. (10') to 7.545 for Eq. (18) which is a difference of only 0.4%.

Let us now consider a Fe-C-Si alloy containing w_C wt.% carbon and w_{Si} wt.% silicon. The mole fractions x_{Fe}, x_C and x_{Si} are calculated and then used to express x_{subst} and M_m^{γ}. Inserting Eq. (13) in Eq. (14) gives:

$$V_m^{\gamma} = \frac{x_{subst} \cdot N_A \cdot \left(a^{\gamma,0} + 8.0344 \cdot 10^{-5} \cdot T_C + 0.01865 \cdot w_C + 0.007019 \cdot w_C^2 - 0.001 \cdot w_{Si}\right)^3}{4} \qquad (19)$$

or, with the use of the value of $a^{\gamma,0} = 3.57344$ Å:

$$V_m^{\gamma} = x_{subst} \cdot V_m^{\gamma,0} \cdot \left(1 + 2.2484 \cdot 10^{-5} \cdot T_C + 0.00522 \cdot w_C + 0.00196 \cdot w_C^2 - 0.00028 \cdot w_{Si}\right)^3 \qquad (19')$$

As all terms other than 1 in the brackets are small, this can be written as well:

$$V_m^{\gamma} \approx x_{subst} \cdot V_m^{\gamma,0} \cdot \left(1 + 6.745 \cdot 10^{-5} \cdot T_C + 0.0157 \cdot w_C + 0.00589 \cdot w_C^2 - 0.00084 \cdot w_{Si}\right) \qquad (20)$$

The specific volume is then given by:

$$v_m^{\gamma} \approx \left(\frac{x_{subst}}{M_m^{\gamma}}\right) \cdot V_m^{\gamma,0} \cdot \left(1 + 6.745 \cdot 10^{-5} \cdot T_C + 0.0157 \cdot w_C + 0.00589 \cdot w_C^2 - 0.00084 \cdot w_{Si}\right) \qquad (21)$$

With the same observation as above that all the terms but 1 in the brackets are small, the density is approximately given by:

$$\rho^{\gamma} \approx \left(\frac{1}{x_{subst}} \cdot \frac{M_m^{\gamma}}{M_m^{Fe}}\right) \cdot 8.129 \cdot \left(1 - 6.745 \cdot 10^{-5} \cdot T_C - 0.0157 \cdot w_C - 0.00589 \cdot w_C^2 + 0.00084 \cdot w_{Si}\right) \qquad (22)$$

As before for the liquid, the linear expansion coefficient β of austenite is given as:

$$\beta = -\frac{1}{3}\cdot\frac{\left(d\rho^{\gamma}/dT\right)}{\rho^{\gamma}} \tag{23}$$

that can be readily calculated at any temperature using Eq. (21) or Eq. (22).

4. Theoretical density change upon cast iron solidification

4.1 Ideal volume change

This section deals with ideal volume change without porosity forming upon solidification, and assuming each of the phases is chemically homogeneous. Solid cast iron is a mixture of graphite and austenite whose density can be expressed as a function of the density of each phase. Let us denote m^{γ} and V^{γ} the mass and volume of austenite in a sample, and m^{g} and V^{g} the mass and volume of graphite in the same sample. The sums $m=m^{\gamma}+m^{g}$ and $V=V^{\gamma}+V^{g}$ are the mass and volume of the whole sample, while the volume and mass fraction of each of the phases ϕ (ϕ: γ for austenite and g for graphite) are defined as $g^{\phi}=V^{\phi}/(V^{\gamma}+V^{g})$ and $f^{\phi}=m^{\phi}/(m^{\gamma}+m^{g})$, respectively. Based on the volume fractions, the density of the solid cast iron, ρ^{castiron}, is written:

$$\rho^{\text{castiron}} = \frac{m^{\gamma}+m^{g}}{V} = \frac{V^{\gamma}}{V}\cdot\frac{m^{\gamma}}{V^{\gamma}} + \frac{V^{g}}{V}\cdot\frac{m^{g}}{V^{g}} = g^{\gamma}\cdot\rho^{\gamma} + g^{g}\cdot\rho^{g} \tag{24}$$

A similar equation can be written using the mass fractions applied to the specific volume that is the inverse of the density:

$$\left(\rho^{\text{castiron}}\right)^{-1} = \frac{V^{\gamma}+V^{g}}{m} = \frac{m^{\gamma}}{m}\cdot\frac{V^{\gamma}}{m^{\gamma}} + \frac{m^{g}}{m}\cdot\frac{V^{g}}{m^{g}} = f^{\gamma}\cdot\left(\rho^{\gamma}\right)^{-1} + f^{g}\cdot\left(\rho^{g}\right)^{-1} \tag{25}$$

If there is no porosity formed, then the volume and mass fractions are such that:

$$g^{\gamma}+g^{g} = 1 = f^{\gamma}+f^{g} \tag{26}$$

Assuming graphite is pure carbon (100 wt.% C) and that austenite is chemically homogeneous, the lever rule applied to carbon gives the mass fraction of graphite and hence that of austenite:

$$f^{g} = 1 - f^{\gamma} = \frac{w_C^0 - w_C^{\gamma}}{100 - w_C^{\gamma}} \tag{27}$$

where w_C^0 is the nominal carbon content of the alloy and w_C^{γ} is the carbon content in austenite (wt.%).

Following Heine [22], it may be assumed that solidification of lamellar cast iron is such that the austenite phase in the eutectic cells gets quickly -during growth- at the composition given by the austenite/graphite equilibrium, that is: $w_C^{\gamma} = w_C^{\gamma/g}$. A first set of calculations were carried out for two eutectic cast irons with 2 wt.% and 4 wt.% Si using the TCFE-8 database to get the carbon content of the eutectic, $w_{C,EUT}$, and its temperature, T_{EUT}, which are listed in Table 1. To illustrate the possibility of solidification with undercooling and the effect of cooling after solidification, the evolution of the liquid density was calculated down to 1100°C and that of austenite in equilibrium with graphite, $w_C^{\gamma/g}$, down to 900°C. Then, calculation of the cast iron density was carried out using the following expression for graphite density [21]:

$$\rho^g = \left(0.4419 + 10.5 \cdot 10^{-6} \cdot T_C\right)^{-1} \qquad (28)$$

Figure 8 shows the change in density with temperature of the liquid, austenite and the cast iron for the two silicon contents. The density of austenite is higher than that of the liquid, which relates to the known shrinkage upon precipitation of this phase. However, it is noticed a decrease of the solid cast-iron density with respect to the corresponding liquid density, which means a theoretical expansion upon solidification. Further, it is seen that the density difference between the liquid and the cast iron is lower for the 4% Si than for the 2% Si, which indicates a lower expansion for the higher as compared to the lower silicon content.

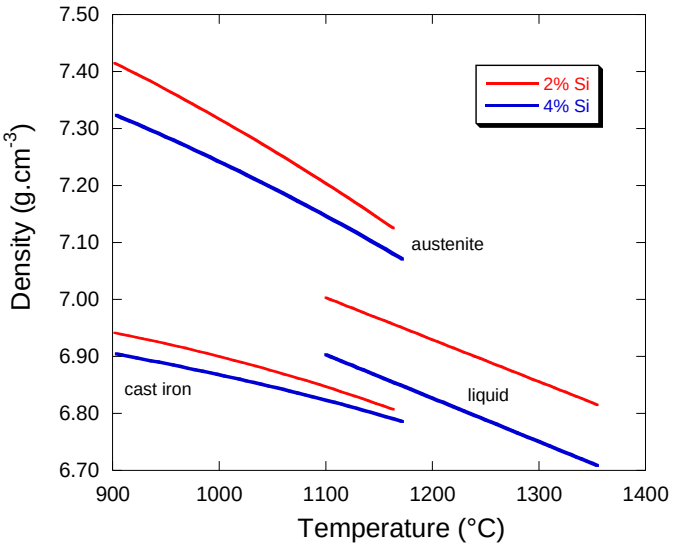

Figure 8. Change with temperature of the density of liquid and solid eutectic cast irons with 2 wt.% Si (thin red lines) and 4 wt.% Si (thick blue lines), and of the austenite in equilibrium with graphite.

Table 1. Data for 2 wt.% Si and 4 wt.% Si alloys calculated with TCFE-8: carbon content of the eutectic, $w_{C,EUT}$, eutectic temperature T_{EUT}, carbon content of austenite at T_{EUT}-15°C when in equilibrium with graphite, $w_C^{\gamma/g}$, and with liquid, $w_C^{\gamma/l}$.

w_{Si} (wt.%)	$w_{C,EUT}$ (wt.%)	T_{EUT}	$w_C^{\gamma/g}$ (wt.%)	$w_C^{\gamma/l}$ (wt.%)
2	3.775	1164.9	1.682	1.748
4	3.247	1172.5	1.319	1.418

For further illustrating the ideal volume change upon solidification of cast irons, the relative change of volume $\Delta V/V$ is calculated as:

$$\Delta V/V = \left(V^{\text{castiron}} - V^{\text{liquid}}\right)/V^{\text{liq}} = \left(\rho^{\text{liq}} - \rho^{\text{castiron}}\right)/\rho^{\text{castiron}} \qquad (29)$$

that is positive in case of expansion upon solidification.

For comparing with Heine's predictions, calculations were performed for solidification with 15°C undercooling with respect to the eutectic temperature, and for nominal carbon content of the cast irons varying from 3.0 to 4.5 wt.%. The values of $w_C^{\gamma/g}$ that were used for these calculations are listed in Table 1 and the predicted values of $\Delta V/V$ are plotted in Fig. 9 with solid lines. This shows expansion values about three times larger than those evaluated by Heine for the LGI case.

Also, Heine suggested that the difference in volume change on solidification between spheroidal graphite cast irons (SGI) and lamellar graphite cast irons (LGI) could be due to the fact that the austenite in SGI has a carbon content dictated by the austenite/liquid equilibrium that relates to a higher carbon content, $w_C^{\gamma/l}$. The values of $w_C^{\gamma/l}$ at 2 wt.% and 4 wt.% Si and a temperature 15°C below T_{EUT} are also listed in Table 1 and the corresponding calculations of $\Delta V/V$ are shown with dotted lines in Fig. 9. In contrast with Heine's calculations, there is very little difference between the calculations with $w_C^{\gamma/g}$ and $w_C^{\gamma/l}$ because the increase of the carbon content in austenite leads to a density decrease of this phase that compensates for the decrease of graphite precipitation. In other words, the difference between LGI and SGI for what concerns solidification shrinkage is not to be found in a change of the austenite carbon content because of growth conditions as postulated by Heine.

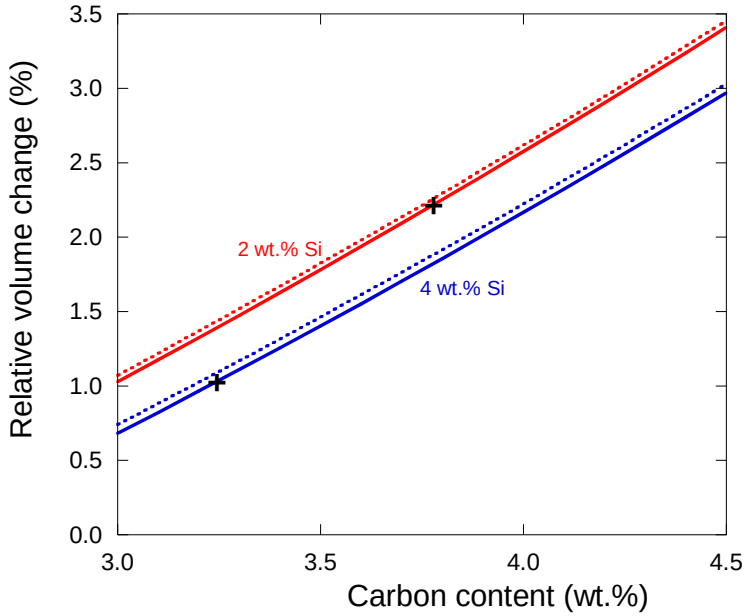

Figure 9. Volume change upon solidification of 2 wt.% Si and 4. wt.% Si cast irons with varying nominal carbon content. Solid lines are for austenite in equilibrium with graphite, dotted lines when in equilibrium with liquid. The crosses show the location of the eutectic.

As a matter of fact, there is a huge amount of reports on shrinkage formation in cast irons that have been regularly reviewed [22, 23]. These reviews reminded the importance of the coupling between mold behavior and the use or not of a riser, and emphasized as well the role of temperature gradients in the solidifying parts, to explain that cast irons have been reported to contract or expand upon solidification. In these lines, studying the volume change of a small cylinder in a non-expandable mold cooling slowly enough to avoid building up of temperature gradients, would appear the most appropriate conditions for comparison with the above ideal case. Such an experiment was reported by Bates et al. [24] who compared the behavior of a eutectic LGI (3.55 wt.% C, 2.40 wt.% Si), a eutectic SGI (3.50 wt.% C, 2.39 wt.% Si) and a hypereutectic SGI (3.64 wt.% C, 2.70 wt.% Si). Most of their experiments were carried out at a cooling rate of 0.1°C/s (6°C/min). Bates et al. observed an expansion for all three alloys, amounting to 1.3% for eutectic LGI, 3.5% for the eutectic SGI and 4% for the hypereutectic SGI. The value for the LGI is very close to the 1.6-1.7% that could be predicted on the basis of Fig. 9, thus giving some support to the present calculations and suggesting this alloy solidified without porosity formation. Kagawe et al. [25] repeated the same type of experiments, though using a higher cooling rate set at 13°C/min. For LGI with various C and Si contents, but yet all hypoeutectic alloys, they reported $\Delta V/V$ values that are slightly higher

than those shown in Fig. 9. More interesting, they observed a decrease of $\Delta V/V$ with an increase of the Si content that correlates perfectly with Fig. 9.
In contrast, the values measured by Bates et al. for the SGI are more than 2 times larger than the expected 1.6-1.7%, suggesting shrinkage porosity appeared in these alloys that have unfortunately not been characterized. Kagawa et al. [25] studied also three SGI with 2.4 wt.% Si and carbon content between 3.0 and 3.6 wt.%. They found a lower $\Delta V/V$ than for LGI, and noticed it decreases with an increase of the carbon content, suggesting the expansion effect due to graphite was overtaken by the shrinkage effect of off-eutectic austenite in these hypoeutectic alloys. More recently, Stefanescu et al. [26] reported results in line with those of Bates et al., with much higher expansion for SGI than for LGI when cast in a mold encased in a steel frame to avoid mold expansion. The much larger expansion of SGI as compared to LGI is certainly to be found in the difference in the growth mechanism and the formation of micro-shrinkage as rationalized by Théret and Lesoult [27] and described in the following section.

4.2 Formation of micro-shrinkage in SGI

Assuming a fully and idealized eutectic microstructure and that no external forces are applied to the solidifying alloy, Fig. 10 compares the evolution of the packing of the eutectic entities for LGI (top row) and SGI (bottom row). After nucleation and independent growth of the eutectic entities within the liquid (column to the left in Fig. 10), a critical solid fraction g_C^s is reached at which a continuous solid skeleton is formed (middle column in Fig. 10). Afterwards, in the case of LGI, austenite and graphite grow side by side within the liquid remaining in between the eutectic cells and the expansion due to the phase change is transmitted to the liquid and then to the whole sample. In the case of SGI, the expansion due to graphite growth is transmitted to the solid skeleton while the remaining liquid recedes to give austenite with a contraction leading to the formation of micro-shrinkage. The column to the right in Fig. 10 illustrates the expected higher expansion of SGI when compared to LGI.
Let V_C be the volume of the sample at the critical volume fraction of liquid, $g_C^l = 1 - g_C^s$, and ΔV_C its increment when the fraction of liquid changes from g_C^l to 0 at solidification completion. Assuming the change of volume is solely due to graphite precipitation, one has:

$$\frac{\Delta V_C}{V_C} = \frac{\Delta V^g}{V_C^s} \qquad (30)$$

in which V_C^s is the volume of solid when the solid skeleton has just formed and ΔV^g is the change of volume of graphite during the last solidification step, i.e. when the liquid fraction decreases from g_C^l to 0. Théret and Lesoult calculated ΔV^g by combining the mass balances of carbon and of substitutional solutes. However, an order of magnitude can be obtained by simply reminding that the ratio of the austenite shell radius to the graphite spheroid radius is 2.4 [28]. One thus have $V^g / V^s = (1/2.4)^3$ and $\Delta V^g / V_C^s \approx g_C^l \cdot (1/2.4)^3$. For a value of g_C^l corresponding to perfect packing, i.e. 0.26, one gets a relative volume change of 1.9% that compares perfectly with the 2.2% difference in expansion between LGI and SGI eutectic alloys reported by Bates et al.

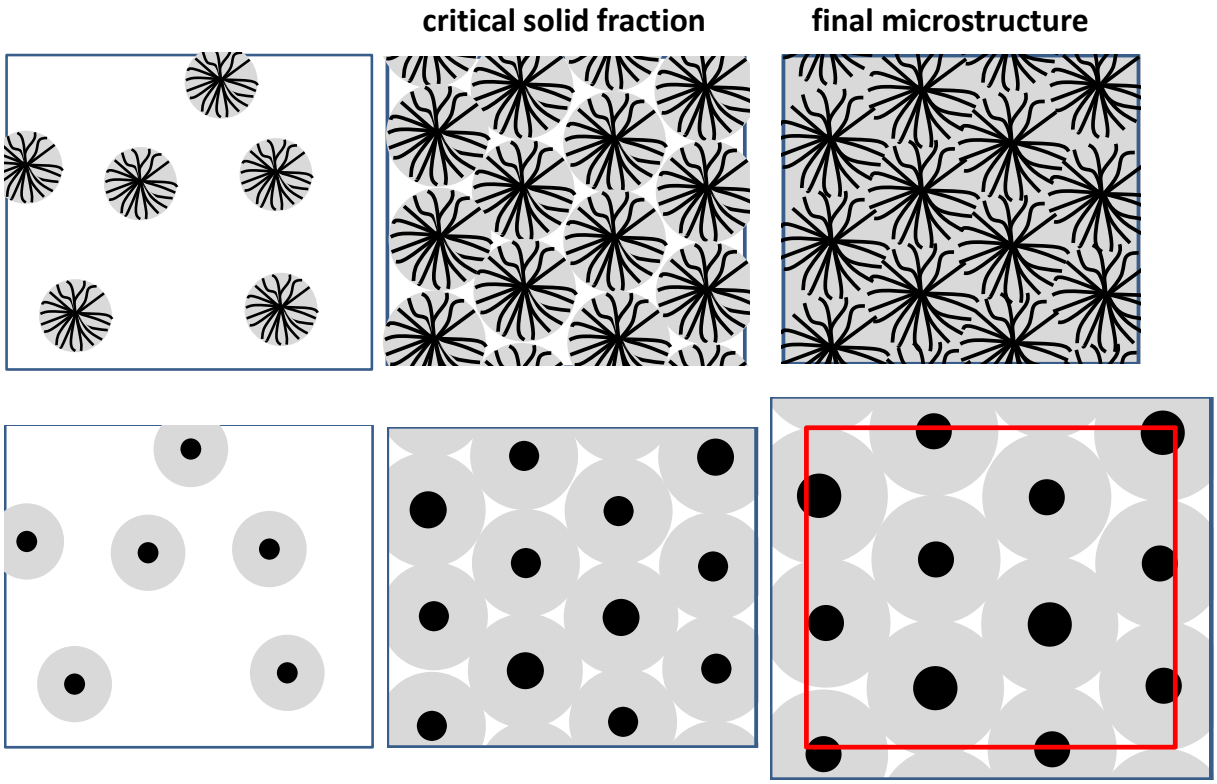

Figure 10. Schematic of microstructure formation in LGI (upper row) and SGI (lower row) illustrating the effect of expansion due to graphite precipitation above the critical solid fraction at which a continuous solid skeleton is formed.

The above description schematized with Fig. 10 assumed that there is no liquid feeding to compensate for the expansion and for the disappearance of the liquid between the eutectic spheres. Indeed, a negative pressure develops in these areas that is a driving force for liquid flow in case there is a riser available. This was not the case in the Bates et al. experiments and

was thus not considered in the present work. For real castings, the presence of risers and of temperature gradients should be considered. In any location, the progress of solidification once the solid skeleton has built up makes the movement of the liquid more and more difficult. This leads to a pressure drop of the liquid moving through the mushy zone that is described by Darcy's law and can be coupled with a description of gas evolution to predict porosity and void formation in any alloys [29, 30] and in particular in cast irons [21, 31].

The idealized microstructure model in Figure 10 gives an estimate of the upper limit of SGI expansion in the case of alloys having a fully eutectic microstructure. For a more quantitative approach of nearly eutectic or slightly hypereutectic alloys, the presence of non-eutectic austenite dendrites should be taken into account. This can be done in accordance with the physical modeling developed by Lesoult et al. [LES98, LAC98] for small castings which has also been applied to thin wall castings [PED06]. The volume change is then a weighted volume average of the contraction of the non-eutectic austenite and the eutectic expansion calculated as above. This physical modeling has been slightly improved by Bjere et al. [BJE18] to take into account the fact that graphite spheroids are distributed in austenite grains bound to off-eutectic dendrites as described by Rivera et al [RIV20]. The predicted expansion will not be affected by this improvement because the total graphite precipitation is unchanged. However, if the porosity calculation were to be performed, the difference in liquid flow between and within the austenite grains would have to be taken into account, as it has been shown that the final porosity is mainly intragranular [RIV20]. The above modeling approach has recently been improved in the case of hypoeutectic SGI by allowing for the free growth of graphite spheroids before being encapsulated by austenite [TEW21]. This allows for a more accurate description of the size distribution of graphite spheroids which has been shown to be important for porosity formation [LEK19], but again will not affect the maximum expansion of the SGI as predicted by the above description with weighting for non-eutectic austenite.

Conclusion

Based on a literature review of the density of Fe and Fe-based alloys, equations giving the density of liquid and austenite of silicon cast irons have been assessed. They have then been used to predict expansion during solidification of cast iron when near-equilibrium is achieved. The predicted expansion agrees with experimental results in the case of lamellar graphite cast iron. In contrast, in the case of spheroidal graphite cast iron, bulging of the solid skeleton must be accounted for to explain the much larger expansion that has been reported. This work

thus provides the density data needed for further studies of shrinkage formation in silicon cast irons in actual casting conditions.

Acknowledgments

Vasile-Lucian Diaconu, Björn Domeij and Attila Dioszegi from JTU university (Sweden) are warmly acknowledged for helping in getting relevant references. We are indebted to the reviewers for their pressure to add some final comments concerning the limits of the idealized model.

Conflict of interest

The authors declare that they have no conflict of interest

References

[1] A. Jablonka, K. Harste and K. Schwerdtfeger, Steel Research 62, 24-33 (1991)

[2] J. Miettinen, Metall. Mater. Trans. B 28, 281-297 (1997)

[3] L.D. Lucas, Mém. Sci. Rev. Métall. 61, 97-116 (1964)

[4] E.J. Ash, C.M. Saeger, Bureau of Standards Journal of Research 8, 601-614 (1932)

[5] T. Yoshikawa, Materials Transactions 54, 1968-1974 (2013)

[6] I. Jimbo, A.W. Cramb, Metall. Trans. B 24, 5-10 (1993)

[7] A. Olsson, Scand. J. Metall. 10, 263-271 (1981)

[8] C. Dumay, A.W. Cramb, Metall. Mater. Trans. B 26, 173-176 (1995)

[9] Yu. M. Gertman, P.V. Gel'd, Russian J. Physical Chemistry 36, 788-792 (1962)

[10] N.K. Dzhemilev, S.L. Popel, B.V. Tsarewskiy, Fiz. Metal. Metalloved 18, 83-87 (1964)

[11] Y. Kawai, K. Mori, M. Kishimoto, Tetsu-to-Hagane 60, 29-37 (1974)

[12] J. Lacaze, O. Dezellus, Metall. Mater. Trans. B 53, 161-177 (2022)

[13] Calculations perfomed with the THERMOCALC software and the TCFE-8 database, https://www.thermocalc.com/

[14] T. Kusakawa, S.Y. Kim, T. Kondo, Report of the Castings Research Laboratory, Waseda University, 1972, vol. 23, pp. 23-32.

[15] K. Hellström, L. Diaconu, A. Dioszegi, China Foundry 17, 127-136 (2020)

[16] L.D. Lucas, Mém. Sci. Rev.Métall. 69, 479-492 (1972)

[17] Z.S. Basinski, W. Hume-Rothery, A.L. Sutton, Proc. Roy. Soc. A 229, 459-467 (1955)

[18] N. Ridley, H. Stuart, Metal Science J. 4, 219-222 (1970)

[19] G.H. Cockett, C.D. Davis, J. Iron Steel Inst., Feb. 1963, 110-115
[20] Qiming Chen, E.W. Langer, O.N. Hansen, Scand. J. Metallurgy 23, 3-8 (1994)
[21] P. Dietrich, G. Lesoult, Simulation of heat transfer and capillary feeding during solidification of sand mold S.G. iron castings, in *State of the art of computer simulation of casting and solidification processes, E-MRS Proceedings*, vol. 34, pp. 225-235 (1986)
[22] R.W. Heine, Trans. Am. Foundry Soc. 96, 413-422 (1988)
[23] M. Hecht, La Santé des Pièces en Fontes à Graphite Sphéroïdal, (ETIF, Sèvres, France, 2008)
[24] C.E. Bates, G.L. Oliver, R.H. McSwain, Trans. Am. Foundry Soc. 85, 289-298 (1977)
[25] A. Kagawa, S. Kiguchi, M. Osada, Trans. Japan Foundrymen's Society 18, 18-23 (1995)
[26] D.M. Stefanescu, M. Moran, S. Boonmee, W.L. Guesser, Proceedings of the 2012 AFS congress, 2012, paper 12-045
[27] J.M. Théret, G. Lesoult, Hommes et Fonderie, February issue, 19-30 (1984)
[28] S.E. Wetterfall, H. Fredriksson, M. Hillert, J. Iron Steel Inst., May issue, 323-333 (1972)
[29] M. Rappaz, J.M. Drezet, M. Gremaud, Metall. Mater. Trans. A 30, 449-455 (1999)
[30] G. Lesoult, Int. J. Cast Metals Research, 22, 2-7 (2009)
[31] E.S. Kweon, D.H. Roh, S.B. Kim, D.M. Stefanescu, Inter. Metalcast. 14, 601-609 (2020)
[32] G. Lesoult, M. Castro, J. Lacaze, Acta Mater. 46, 983–995 (1998)
[33] J. Lacaze, G. Lesoult, M. Castro, Acta Mater. 46, 997–1010 (1998)
[34] K.M. Pedersen, J.H. Hattel, N. Tiedje, Acta Mater. 54, 5103–5114 (2006)
[35] M.K. Bjerre, M.A. Azeem, N.S. Tiedje, J. Thorborg, P.D. Lee, J.H. Hattel, Model. Simul. Mater. Sci. Eng. 26, 085012 (2018)
[36] G. Rivera, P.R. Calvillo, R. Boeri, Y. Houbaert, J. Sikora, Inter. J. Metalcast. 14(4), 1172 (2020)
[37] U. Tewari et al., Metall. Mater. Trans. B 52B, 633 (2021)
[38] N. Lekakh, X. Zhang, W. Tucker, H.K. Lee, T. Selly, J.D. Schiffbauer, Mater. Charact. 158, 109991 (2019)

Appendix A - Values selected for comparing Fe-Si data from various works

Table 2. Reference, silicon content, density values and measurement method.

	Silicon content (wt.%)	1250°C	1300°C	1350°C	1400°C	1450°C	1500°C	1550°C	1600°C	1650°C	1700°C	Method
Gertman and Gel'd [9]	5.0 9.5 17.5						6.85 6.70 6.45					Weighing
Lucas [3]	2.06							6.80	6.76	6.73	6.69	Bubble pressure
Dzhemilev et al. [10]	5.01 9.94							6.77 6.37				Sessile drop
Kawai et al. [11]	2 5 10							6.77 6.71 6.34				Sessile drop
Olsson [7]	0.83 1.84 4.73							6.876 6.870	6.873 6.823 6.646	6.974 6.779 6.595	6.782 6.566	Bubble pressure
Dumay and Cramb [8]	16.03 18.10					6.039 5.784						Sessile drop
Yoshikawa [5]	17.73 (1) 17.73 (2)	6.086 6.086	6.122 6.032	6.021 6.052	6.031 5.988	5.988 6.031						Bubble pressure

Appendix B - Composition of the Fe-30 at.% Si alloy saturated in carbon [5]

In a study dedicated to surface tension of Fe-Si and Fe-Si-C alloys, Yoshikawa used Fe-Si alloys that were then carbon saturated at various temperatures to give Fe-Si-C alloys. In the present work, data for a Fe-Si alloy with 30 at.% Si were considered. Carbon saturation of this alloy was carried out in graphite crucibles leading to a change in composition of the melt that was calculated using the TCFE-8 database. The results of these calculations are given in mass percent in Table 3 where are also listed the experimental and calculated values of the density.

Table 3. Composition of Fe-30 at.% Si alloy after carbon saturation in graphite crucibles, and experimental and calculated values of the density.

Temperature (°C)	Carbon (wt.%)	Silicon (wt.%)	Experimental density	Density calculated with Eq. (7)
1250	1.33	14.15	6.105	6.260
1300	1.48	14.13	5.989	6.208
1350	1.63	14.11	5.956	6.158
1400	1.79	14.09	5.919	6.107
1450	1.95	14.07	5.902	6.058

Appendix C - Data from Ash and Saeger [4]

Ash and Saeger measured the specific volume of a series of liquid cast irons and plotted them in their Fig. 1. These results have been picked up from their figure and are replotted in Fig. C1. Some of the melts were duplicates and the corresponding results were given without being differentiated (e.g. alloys III and IV in Fig. C1). Table 4 lists the compositions of the alloys studied by Ash and Saeger, selecting however only one of the compositions in case of duplicates. In the original figure by Ash and Saeger, lines were drawn through the data that were nearly but not exactly parallel, while the choice was made to plot parallel lines in Fig. C1.

As it can be noticed in Table 4, the alloys contained different amounts of phosphorus, suggesting checking the effect of this element as assessed in the main text. The comparison of the densities calculated with Eq. (7) without the P terms and the experimental ones in Fig. C2 shows an agreement that could appear satisfactory, with a difference of less than 1.5%. However, accounting for P gave an agreement at better than 0.7% as seen in Fig. C3.

Table 4. Composition of the alloys studied by Ash and Saeger (wt.%)

Melt number	Total carbon	Silicon	Manganese	Phosphorus
III	3.08	1.68	0.44	0.35
VI	2.29	1.24	0.35	0.27
VII	3.76	2.10	0.54	0.46
VIII	3.63	2.87	0.59	0.68
X	2.00	0.85	0.25	0.14
XII	1.97	1.50	0.27	0.14
XIII	3.27	2.87	0.52	0.59
XIV	2.89	2.88	0.44	0.66

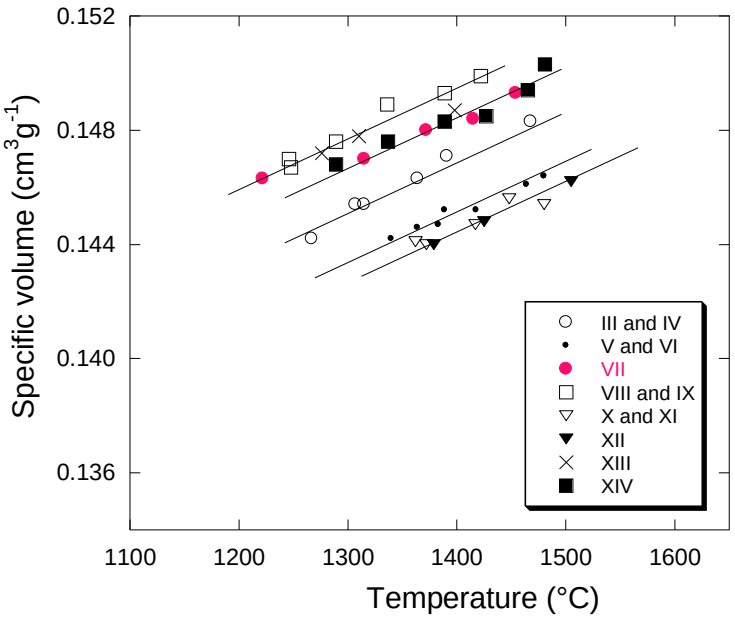

Figure C1. Change with temperature of the specific volume of liquid cast irons studied by Ash and Saeger.

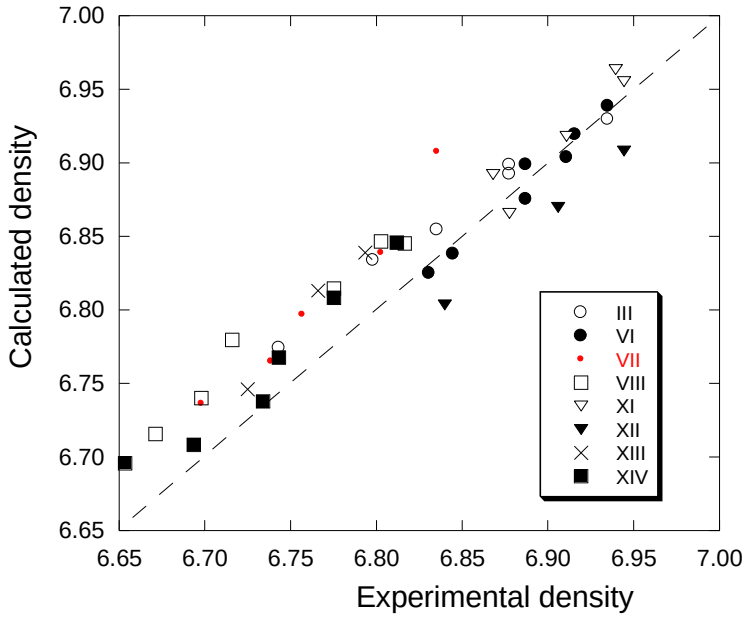

Figure C2. Calculated versus experimental density values when P is not accounted for in Eq. (7). The dashed line is the bisector.

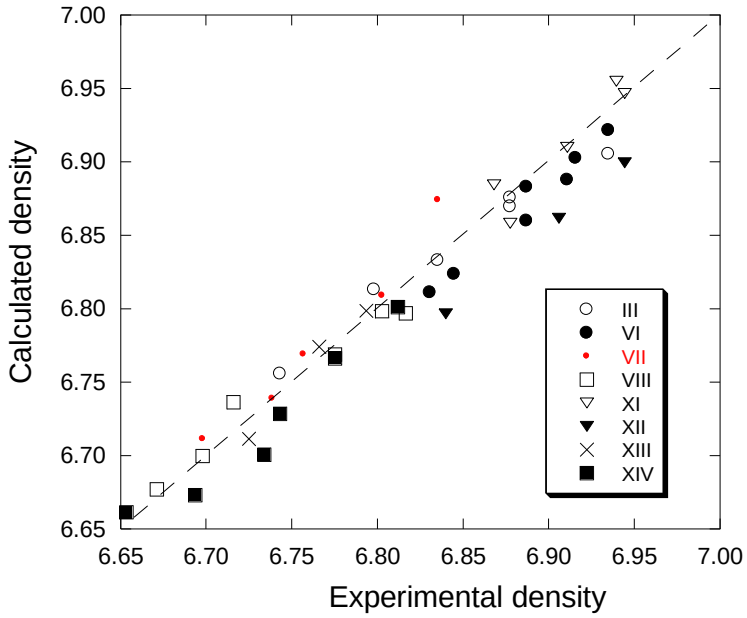

Figure C3. Calculated versus experimental density values when P is accounted for in Eq. (7). The dashed line is the bisector.